J. Fluid Mech. (1967), *vol.* 28, *part* 1, *pp.* 113–129
Printed in Great Britain

Potential flow about two-dimensional hydrofoils

By JOSEPH P. GIESING AND A. M. O. SMITH
Douglas Aircraft Company, Aircraft Division, Long Beach, California

(Received 15 November 1965 and in revised form 6 June 1966)

This paper describes a very general method for determining the steady two-dimensional potential flow about one or more bodies of arbitrary shape operating at arbitrary Froude number near a free surface. The boundary condition of zero velocity (solid wall) or prescribed velocity (suction or blowing) normal to the body surface is satisfied exactly, and the boundary condition of constant pressure on the free surface is satisfied using the classic small-wave approximation. Calculations made by the present method are compared with analytic results, other theoretical calculations and experimental data. Examples for which no comparison exists are also presented to illustrate the capability of the method.

1. Introduction

The pressure distribution and flow field about hydrofoils or systems of hydrofoils is important for several reasons: the determination of cavitation inception, the calculation of boundary-layer characteristics, and the determination of the inviscid hydrodynamic characteristics—lift, moment, and wave resistance. Thin hydrofoil theory (Keldysch & Lawrentjew 1935; Walderhaug 1964) predicts pressures that are physically unrealistic at the hydrofoil nose (usually infinite) and unusable either for the determination of cavitation or for the calculation of boundary-layer characteristics. Other theories, some based on conformal-mapping techniques (Havelock 1936; Kochin 1937; Nishiyama 1957) are restricted to single bodies. Two theories that do consider the flow about more than one body are given by Coombs (1950) and Isay (1960), but both of these are only approximate.

This paper presents a method that determines the flow about one or more large-aspect-ratio hydrofoils, of arbitrary shape, moving with constant forward speed and at arbitrary Froude number. The Neumann boundary condition on the surfaces of the hydrofoils, that is, zero velocity (solid wall) or prescribed velocity normal to solid boundaries (suction or blowing), is satisfied exactly by a surface source distribution that also satisfies the classic small-perturbation free-surface boundary condition.

The techniques on which the present method is based (Smith & Pierce 1958) are not restricted to two-dimensional flow, and therefore an extension to include three-dimensional problems such as the flow about submarines and ships may be possible (see also Hess & Smith 1964). In addition, it seems possible to refine the method to include higher order terms in the free-surface boundary condition.

2. Description of the problem

The problem of concern is the uncavitated two-dimensional potential flow past one or more bodies moving with constant forward speed beneath a free surface. Since the potential-flow model is used and surface tension effects neglected, the governing equations of fluid motion and pressure are the Laplace and Bernoulli equations, respectively. They are

$$\nabla^2\Phi = 0, \tag{1}$$

$$p/\rho + \tfrac{1}{2}\mathbf{V}.\mathbf{V} + gy = p_\infty/\rho + \tfrac{1}{2}U_\infty^2, \tag{2}$$

with

$$\mathbf{V} = \nabla\Phi.$$

The symbols $\mathbf{V}, \Phi, p, \rho$ and g are the velocity, potential, pressure, mass density and acceleration due to gravity, respectively and the subscript ∞ refers to infinity upstream at the free surface.

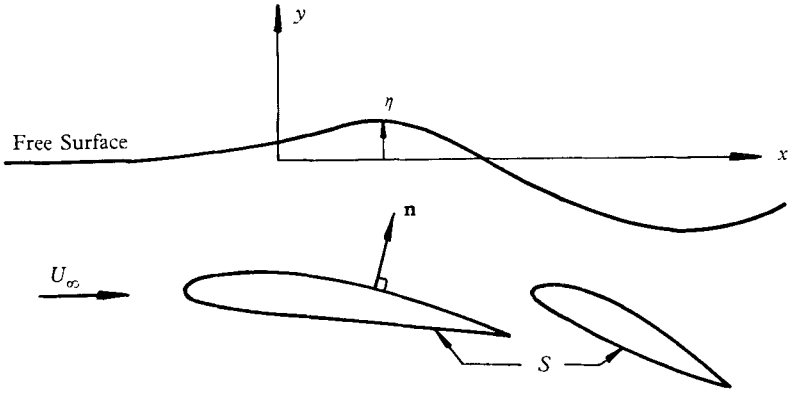

FIGURE 1. Schematic diagram.

The fluid is assumed to occupy the lower half-plane and to be bounded by a free surface upon which the pressure is constant. Figure 1 shows the co-ordinate system and direction of fluid motion. Boundary conditions must be applied to the surfaces S of the hydrofoils and to the free surface. The boundary condition applied at the hydrofoil surfaces requires that the velocity normal to the surfaces either be zero (solid body) or be prescribed (suction or blowing). After the introduction of the disturbance potential ϕ, defined by

$$\Phi = U_\infty x + \phi, \tag{3}$$

the boundary condition on the hydrofoil surfaces can be written

$$\frac{\partial\phi}{\partial n} = -U_\infty \mathbf{i}.\mathbf{n} + f(S) \quad \text{on} \quad S, \tag{4}$$

where S defines the hydrofoil surfaces, $\mathbf{n}$ the outward normal vector and $f(S)$ the blowing or suction velocity.

The boundary condition on the free surface requires that the pressure be constant and that the free surface $y = \eta(x)$ be a streamline. It can be shown that the resulting boundary condition is exactly

$$\left[U_\infty + \frac{\partial\phi}{\partial x}\right]\left[\frac{\partial^2\phi}{\partial x^2}\left(U_\infty + \frac{\partial\phi}{\partial x}\right) + \frac{\partial\phi}{\partial y}\frac{\partial^2\phi}{\partial x\partial y}\right] + g\frac{\partial\phi}{\partial y} = 0 \quad \text{on} \quad y = \eta(x). \tag{5}$$

This condition is non-linear in the potential ϕ, and it is applied to a surface that is not known *a priori*. The last boundary condition that must be applied expresses the physically observed fact that the disturbance velocities due to the ensemble of hydrofoils vanish only far upstream and far below the foils, that is,

$$\left.\begin{aligned} \nabla\phi \to 0 \quad &\text{when} \quad x \to -\infty, \\ \nabla\phi \to 0 \quad &\text{when} \quad y \to -\infty. \end{aligned}\right\} \tag{6}$$

A disturbance downstream ($x > 0$) is observed in the form of trailing surface waves that apparently would extend to infinity were it not for the effects of viscosity.

Simplification of the free-surface boundary condition

The problem as posed is highly intractable, because of the free-surface boundary condition (5). Since this boundary condition is non-linear and is applied to a surface that is not known, some simplification of this boundary condition is needed. A linear boundary condition applied at the undisturbed surface $y = 0$ is obtained from (5) if the wave heights and disturbance velocity at the free surface are assumed to be small compared to the characteristic length ℓ (usually body chord length) and the forward speed U_∞, respectively. (5) then becomes

$$\partial^2\phi/\partial x^2 + \nu(\partial\phi/\partial y) = 0 \quad \text{on} \quad y = 0, \tag{7}$$

where $\nu = g/U_\infty^2$. With these same assumptions, (2) furnishes an expression for the linearized wave height. Thus

$$\eta = -\frac{1}{\nu}\frac{\partial\phi(x,0)}{\partial x}\Big/U_\infty. \tag{8}$$

(7) is also obtained as the lowest order term in an expansion of (5) when ϕ and η are expanded in terms of some small parameter ϵ (Wehausen & Laitone 1960). The only requirement for ϵ is that ϕ vanish in the region of the free surface when ϵ vanishes. It is proposed here to consider this expansion in terms of ℓ/h where h is hydrofoil submergence depth. The first term of the expansion is to satisfy the boundary condition on the body surface exactly, that is, satisfy (4). The rest of the terms are to satisfy a homogeneous boundary condition on the body surface, that is, satisfy (4) with the right-hand side set equal to zero.

If the depth is sufficiently large, terms of higher order than ϵ can be retained, which increases the accuracy. For the present, only the first-order term (7) is used, since it offers a practical solution for all but extreme cases and presents no convergence difficulties.

In what is to follow the characteristic non-dimensional parameter is the Froude number. The Froude number is defined in (9) as follows

$$Fr = U_\infty(g\ell)^{-\frac{1}{2}}. \tag{9}$$

3. Solution

The problem to be solved is reduced to finding the solution of the Laplace equation that is consistent with the boundary conditions given by (4), (6) and (7) and which satisfies the Kutta condition on each body, if applicable. First, an elementary solution of the Laplace equation is assumed, of the form

$$G(P,Q) = \ln[r(P,Q)] + K(P,Q).$$

The first term on the right is the familiar potential at P due to a unit source at Q. The second term is a function, non-singular in the region of interest, that causes $G(P, Q)$ to satisfy the free surface, radiation and far-field boundary conditions. The radiation and far-field boundary conditions are given by (6). The function $G(P, Q)$ will be called a source because of its close relation to the usual simple source. Starting with Green's third identity and using the source $G(P, Q)$ in place of the usual source potential, the following equation can be obtained (see Lamb 1932, p. 60),

$$\phi(P) = \frac{1}{2\pi}\int_S \sigma(q)\, G(P, q)\, dS; \tag{10}$$

that is, $\phi(P)$ is the potential at a general point P due to a distribution, on the surface S, of sources of strength $\sigma(q)$. The value of Q on the body surfaces is called q.

Since an expression for the potential, (10), is known, the boundary condition on the body surface, (4), may be written as follows

$$\frac{\partial\phi(p)}{\partial n} = -U_\infty \mathbf{i}.\mathbf{n}(p) = \lim_{P\to p}\frac{1}{2\pi}\int_S \sigma(q)\,\nabla G(P, q).\mathbf{n}(P)\, dS, \tag{11}$$

with the assumption of no flow through the hydrofoil surface (suction or blowing). Here p is a point on S. If the limit is taken in (11) and the principal part abstracted from the integral, then the result is a non-singular Fredholm integral equation of the second kind for the unknown source strength σ. For convenience the limit will not be taken and the integral of (11) will be left in its present form.

(11) then insures that the Neumann boundary condition (4) is satisfied. The function $K(P, Q)$ must now be found such that $G(P, Q)$ satisfies the free-surface condition (7) and the radiation condition (6). Note that if the individual source potential $G(P, Q)$ satisfies (6) and (7), an entire distribution of such sources will also satisfy (6) and (7), since these boundary conditions are linear and homogeneous. From Kochin, Kibel & Roze (1964), we obtain $K(P, Q)$ as

$$K(P, Q) = \mathrm{Re}\left[\ln(z-\bar{c}) - 2\,e^{-i\nu z}\int_{-\infty}^{z}\frac{e^{i\nu t}}{t-\bar{c}}\,dt\right], \tag{12}$$

where z and c are the complex co-ordinates of P and Q, respectively, and the bar indicates the conjugate. It is convenient at this point to introduce the complex potential F such that $G = \mathrm{Re}(F)$ and $dF/dz = \partial G/\partial x - i\,\partial G/\partial y$. Here F is

$$F(z, c) = \ln(z-c) + \ln(z-\bar{c}) - 2\,e^{-i\nu z}\int_{-\infty}^{z}\frac{e^{i\nu t}}{t-\bar{c}}\,dt. \tag{13}$$

The integral in (13) can be put into more convenient form by transformation using the relation

$$\nu(t-z) = -k(z-\bar{c})$$

and then separating the principal part. The result is

$$F(z, c) = \ln(z-c) + \ln(z-\bar{c}) + 2\mathrm{PV}\int_0^\infty \frac{e^{-ik(z-\bar{c})}}{k-\nu}\,dk - 2\pi i\, e^{-i\nu(z-\bar{c})}, \tag{14}$$

where PV means the principal value. Introduction of the real part of (14) into (11) leads to an integral equation for the unknown source distribution σ that satisfies

the Neumann boundary condition on the body surface (4), the linearized free-surface condition (7), and the radiation condition (6). Only the Kutta condition is left to consider.

To satisfy the Kutta condition on each of the bodies, additional solutions must be obtained that satisfy the conditions (6) and (7) but are homogeneous in the Neumann boundary condition (4), that is, solutions where $\partial\phi/\partial n = 0$ on S. Any number of these solutions may be added to the solution given by (11) without violating (4). Specifically, one such solution is needed for each body to which a Kutta condition is applied. The only non-trivial solution that satisfies these conditions and is also non-singular within the fluid is a circulatory-flow solution about any one of the bodies. The circulation or cyclic constant is arbitrary. One such solution must be obtained for each body that can maintain a circulation. The cyclic constants associated with the bodies are adjusted, since they are arbitrary, until the Kutta condition on each body is satisfied.

A solution that produces a circulation about a particular body is obtained by placing a vortex or distribution of vorticity within the body to produce the desired circulation and by cancelling the resulting flow normal to the body surface with a source distribution. The vortex or distribution of vorticity must, of course, satisfy the boundary conditions (6) and (7), just as the source distribution satisfies it. The potential for such a vortex is

$$\phi_\Gamma = \mathrm{Re}\,\frac{i\Gamma}{2\pi}\left[\ln(z-c) - \ln(z-\bar{c}) - 2\mathrm{PV}\int_0^\infty \frac{e^{-ik(z-\bar{c})}}{k-\nu}\,dk + 2\pi i\, e^{-i\nu(z-\bar{c})}\right], \tag{15}$$

where Γ is the circulation or cyclic constant. If $\partial\phi_\Gamma/\partial n$ denotes the velocity generated by the gradient of (15) normal to and at the body surface, then the source distribution σ_Γ that cancels this velocity is given by the integral equation (11) with $U_\infty \mathbf{i}.\mathbf{n}(p)$ replaced by $\partial\phi_\Gamma(p)/\partial n$.

Solution of the integral equation

The integral equation to be solved, (11), can be written

$$-V_n(p) = \lim_{P\to p}\frac{1}{2\pi}\int_S \sigma(q)\,\nabla G(P,q).\mathbf{n}(P)\,dS, \tag{16}$$

where V_n can represent either $U_\infty \mathbf{i}.\mathbf{n}$ or $\partial\phi_\Gamma/\partial n$, and $G(P,Q)$ is given by the real part of (14). For blowing or suction cases, $f(S)$ must be added to $U_\infty \mathbf{i}.\mathbf{n}$. If the integral in (16) is split into a sum of integrals whose range of integration, ΔS, is small enough so that source strength, σ, can be assumed constant across that range, then (16) can be written approximately as

$$-V_n \approx \lim_{P\to p}\frac{1}{2\pi}\sum_{k=1}^{N}\sigma_k\int_{S_k-\Delta S_k/2}^{S_k+\Delta S_k/2}\nabla G(P,q).\mathbf{n}(P)\,dS. \tag{17}$$

There are now N unknown source strengths σ_k. To obtain N equations, (17) is made to hold at N points on the body surface. The points selected are the mid-points of the elements, that is, p_j. The surface co-ordinates of p_j are S_j. (17) then becomes

$$-V_{n_j} = \sum_{k=1}^{N}\sigma_k A_{jk}, \quad \text{where} \quad A_{jk} = \frac{1}{2\pi}\mathbf{n}_j.\left[\lim_{P\to p_j}\int_{S_k-\Delta S_k/2}^{S_k+\Delta S_k/2}\nabla G(P,q)\,dS\right]. \tag{18}$$

The first half of (18) represents N equations in N unknowns and may be solved using standard matrix techniques once the influence coefficients A_{jk} are known.

To be consistent with the approximation of constant source strength over the element, the element is approximated by a flat segment (see figure 2). The above approximations become exact in the limit as $N \to \infty$. To enable the limit indicated in (18) to be taken, the integration is performed analytically for arbitrary P. In

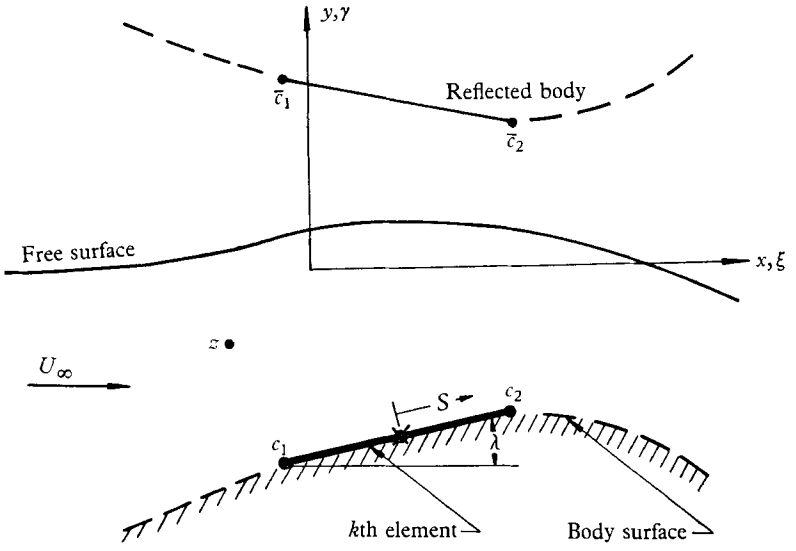

FIGURE 2. Typical flat-surface source element and its reflexion.

performing this integration it is convenient to use complex variables; specifically, the complex potential F is used in place of G. The following relations hold between the vector and complex forms:

$$\nabla G = \mathbf{i}(Re\, dF/dz) + \mathbf{j}(-Im\, dF/dz), \quad \mathbf{I}_{v_k} = \mathbf{i}(Re\, I_k) + \mathbf{j}(-Im\, I_k), \tag{19}$$

where $\mathbf{I}_{v_k}$ represents the integral found in (18) and I_k is its complex equivalent. If only the kth element is considered, the subscript k may be dropped and I may be written as

$$I = \int_{S-\Delta S/2}^{S+\Delta S/2} \frac{dF}{dz}\, dS. \tag{20}$$

From figure 2 the following relations are evident

$$dS = dc\, e^{-i\lambda} = d\bar{c}\, e^{i\lambda}. \tag{21}$$

By means of (21) and (14), (20) becomes

$$\begin{aligned} I &= e^{-i\lambda} \int_{c_1}^{c_2} \frac{dc}{z-c} + e^{i\lambda} \int_{\bar{c}_1}^{\bar{c}_2} \left\{ \frac{1}{z-\bar{c}} + 2\mathrm{PV} \int_0^\infty \frac{-ik\, e^{-ik(z-\bar{c})}}{k-\nu}\, dk - 2\pi\nu\, e^{-i\nu(z-\bar{c})} \right\} d\bar{c} \\ &= e^{-i\lambda} \ln\left(\frac{z-c_1}{z-c_2}\right) + e^{i\lambda} \left\{ \ln\left(\frac{z-\bar{c}_1}{z-\bar{c}_2}\right) + 2\left[\mathrm{PV} \int_0^\infty \frac{e^{-ik(z-\bar{c}_1)}}{k-\nu}\, dk - \mathrm{PV} \int_0^\infty \frac{e^{-ik(z-\bar{c}_2)}}{k-\nu}\, dk \right] \right. \\ &\qquad \left. - 2\pi i [e^{-i\nu(z-\bar{c}_1)} - e^{-i\nu(z-\bar{c}_2)}] \right\}. \end{aligned} \tag{22}$$

The integrals left to evaluate, which are of the form

$$\mathrm{PV}\int_0^\infty \frac{e^{-ik(z-\bar{c})}}{k-\nu}\,dk,$$

can be handled by using contour integration in the complex k-plane. With reference to figure 3, the desired integral can be written

$$\mathrm{PV}\int_0^\infty \frac{e^{-ik(z-\bar{c})}}{k-\nu}\,dk = \int_1 + \int_3 \frac{e^{-ik(z-\bar{c})}}{k-\nu}\,dk = -\int_2 - \int_4 - \int_5 \frac{e^{ik(z-\bar{c})}}{k-\nu}\,dk \qquad (23)$$

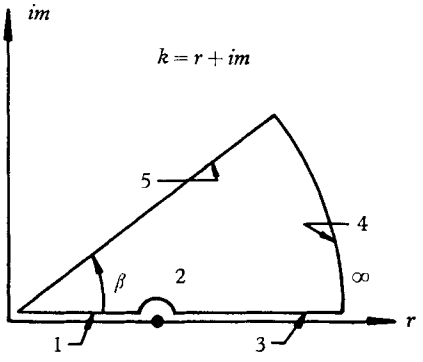

FIGURE 3. Integration contour in the complex k-plane.

since the total contour encloses no singularities. It is possible to find an angle β such that the exponent of $e^{-ik(z-\bar{c})}$ is purely real along contour 5 and such that the integral along contour 4 vanishes. Thus it is found that

$$\beta = \tan^{-1}\left(\frac{x-\xi}{y+\gamma}\right)$$

with $\bar{c} = \xi - i\gamma$ and $z = x + iy$. Note that the sign of β is determined by the sign of $-(x-\xi)$, since both y and γ are negative.

The integral along contour 2 is known once the sign of β is known,

$$-\int_2 \frac{e^{-ik(z-\bar{c})}}{k-\nu}\,dk = (\mathrm{sgn}\,\beta)\,\pi i\, e^{-i\nu(z-\bar{c})}. \qquad (24)$$

The integral along contour 5 is evaluated when the exponential is real, that is, with $k = r(1 + i\tan\beta)$, which gives

$$-\int_5 \frac{e^{-ik(z-\bar{c})}}{k-\nu}\,dk = \int_0^\infty \frac{e^{-u}}{u - i\nu(z-\bar{c})}\,du = e^{-i\nu(z-\bar{c})}E_1[-i\nu(z-\bar{c})], \qquad (25)$$

where E_1 is the exponential integral. Hess & Smith (1966) present a rapid and accurate method for the evaluation of the exponential integral. Here

$$u = r\left\{\frac{(y+\gamma)^2 + (x-\xi)^2}{-(y+\gamma)}\right\}.$$

Substituting the expressions for the integrals in (24) and (25) into (23) gives

$$\mathrm{PV}\int_0^\infty \frac{e^{-ik(z-\bar{c})}}{k-\nu}\,dk = (\mathrm{sgn}\,\beta)\,\pi i\, e^{-i\nu(z-\bar{c})} + e^{-i\nu(z-\bar{c})}E_1[-i\nu(z-\bar{c})]. \qquad (26)$$

Substituting the value of the integral in (26) into (22) completes the evaluation of I. (See Smith, Giesing & Hess 1963 for further details.)

$$I = e^{-i\lambda}\ln\left(\frac{z-c_1}{z-c_2}\right) + e^{i\lambda}\left\{\ln\left(\frac{z-\bar{c}_1}{z-\bar{c}_2}\right) + 2\,e^{-i\nu(z-\bar{c}_1)}E_1[-i\nu(z-\bar{c}_1)]\right.$$
$$\left. - 2\,e^{-i\nu(z-\bar{c}_2)}E_1[-i\nu(z-\bar{c}_2)] - 4\pi i[\delta_1 e^{-i\nu(z-\bar{c}_1)} - \delta_2 e^{-i\nu(z-\bar{c}_2)}]\right\}, \quad (27)$$

where
$$\delta_1 = \begin{cases} 0, \beta_1 > 0 & (z \text{ upstream of } c_1), \\ 1, \beta_1 < 0 & (z \text{ downstream of } c_1), \end{cases}$$
$$\delta_2 = \begin{cases} 0, \beta_2 > 0 & (z \text{ upstream of } c_2), \\ 1, \beta_2 < 0 & (z \text{ downstream of } c_2). \end{cases}$$

The quantities z, c_1 and c_2 are shown in figure 2. The expression for I in (27) may be used in (18) with the aid of (19) to produce an expression for the influence coefficients A_{jk}.

Velocity and pressure field

The velocity or the potential field is easily found once the source distribution over the bodies is known. The disturbance velocity at any point P due to a source distribution is obtained by taking the gradient of (10). The onset flow must be added to this disturbance field to produce the total velocity field. Let the subscript 0 denote circulation-free flow and the subscript Γ denote pure circulatory flow. Then for circulation-free flow the total velocity is

$$\mathbf{V}_0(P) = \nabla\Phi_0 = \nabla(U_\infty x + \phi_0) = U_\infty \mathbf{i} + \int_S \sigma_0(q)\,\nabla G(P,q)\,dS. \quad (28)$$

For a pure circulatory flow the velocity field is

$$\mathbf{V}_\Gamma(P) = \Gamma\left\{\nabla\phi_\Gamma + \int_S \sigma_\Gamma(q)\,\nabla G(P,q)\,dS\right\}, \quad (29)$$

where Γ is the circulation or cyclic constant. The integrals of (28) and (29) are evaluated with the same approximations as the integrals of (16). Therefore

$$\int_S \sigma(q)\,\nabla G(P,q)\,dS \approx \sum_{k=1}^{N} \sigma_k \mathbf{I}_{v_k}(P), \quad (30)$$

where $\mathbf{I}_{v_k}$ is given by (19) and (27). As was mentioned before, there is one circulatory flow associated with each body which causes a circulation about that body alone. A combination of these circulatory flows with the non-circulatory flow produces the total velocity field

$$\mathbf{V}(P) = \mathbf{V}_0(P) + \Gamma_1\mathbf{V}_{\Gamma_1}(P) + \Gamma_2\mathbf{V}_{\Gamma_2}(P) + \ldots + \Gamma_R\mathbf{V}_{\Gamma_R}(P), \quad (31)$$

where R is the number of bodies that can maintain a circulation. The cyclic constants $\Gamma_1, \Gamma_2, \ldots, \Gamma_R$ are adjusted to satisfy the Kutta condition at each of the hydrofoil trailing edges by requiring that the velocity at the trailing edge elements, i.e. the one above and the one below, be equal. The point P is arbitrary and need not be on the body surfaces. Thus the entire flow on or off the body surface is determined.

The pressure can be obtained from (2). A pressure coefficient is defined as follows:

$$C_P = (p - p_\infty + \rho g y)/\tfrac{1}{2}\rho U_\infty^2 = 1 - \mathbf{V}.\mathbf{V}/U_\infty^2, \tag{32}$$

where the term $\rho g y$ is purely hydrostatic. The forces and moments are easily found after the pressure is known by direct integration as follows:

$$C_R = \int_S -C_P \mathbf{n}.\mathbf{i}\, dS, \tag{33a}$$

$$C_L = \int_S -C_P \mathbf{n}.\mathbf{j}\, dS, \tag{33b}$$

$$C_m = \int_S C_P(\mathbf{n}\times\mathbf{r})\, dS,$$

where $\mathbf{r}$ is the position vector from the moment reference point to a surface point. These integrals are evaluated approximately using the trapezoidal rule, that is, summing element by element.

4. Calculated results

Special cases

Two special cases of the theory exist when the hydrofoil operates at an infinite depth or when it operates at a Froude number of zero. These cases correspond to an airfoil in an unrestricted fluid and in ground effect, respectively. They are special because the non-linear boundary condition on the free surface is satisfied exactly.

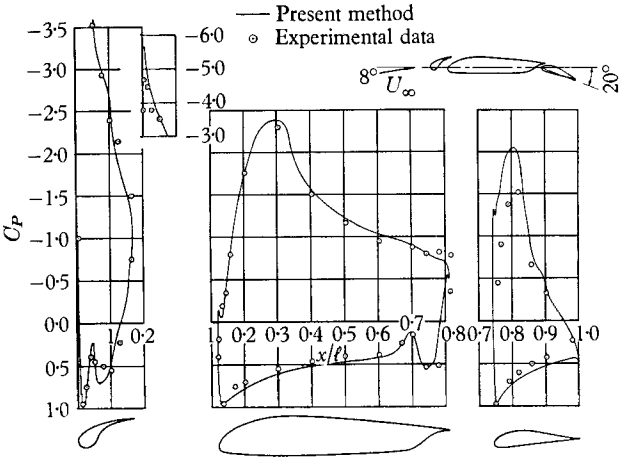

FIGURE 4. Comparison of calculated and experimental pressure distributions on a NACA 23012 airfoil with fixed slot and slotted flap at 8° angle of attack. $C_L = 2{\cdot}26$.

As an example of a hydrofoil at infinite depth, figure 4 shows a comparison of the calculated and experimental pressure distribution on an airfoil with a fixed slot and slotted flap. The experimental data were obtained by Harris & Lowry (1942). The agreement is good except over a part of the lower surface of the slot where the flow is apparently separated. In all cases the force coefficients shown are those calculated by the present method.

As an example of the second special case, figure 5 presents a comparison of the analytic and calculated pressure distribution on a hydrofoil operating at a Froude number of zero. The analytic solution was developed by Giesing (1966). The agreement is good.

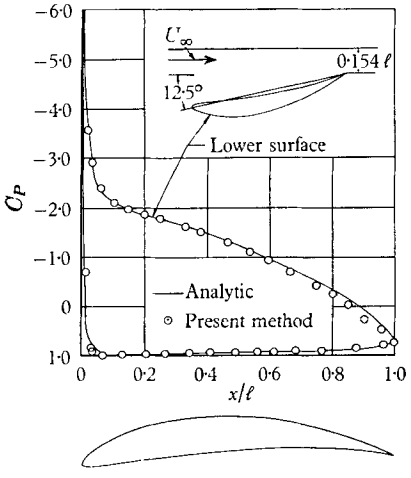

FIGURE 5

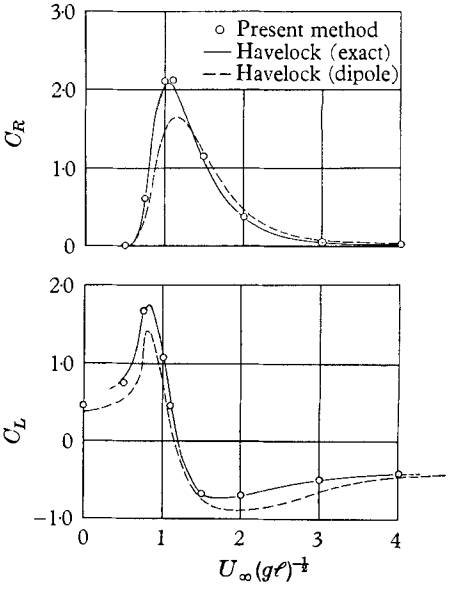

FIGURE 6

FIGURE 5. Comparison of analytic and calculated pressure distributions on a hydrofoil operating at $Fr = 0$. $C_L = -2{\cdot}11$.

FIGURE 6. Comparison of lift and drag coefficients of a circular cylinder as calculated by the present method and as calculated by Havelock. Results for a dipole are also shown.

Comparison with other methods and experimental data

One of the first calculations of the forces on a body under a free surface was for a circular cylinder. Havelock (1928) derived expressions for the lift and drag of a dipole under a free surface, which were assumed to apply to a circular cylinder. Later (1936), he presented the exact solution for the circular cylinder. Figure 6 is a comparison of the wave-resistance coefficient, C_R, and lift coefficient, C_L, of a circular cylinder, as calculated by the present method and as given by Havelock, and for a dipole as given by Havelock. The lift and drag coefficients are defined as the lift and drag divided by $\rho U_\infty^2 \ell/2$ where ℓ, in this case, is the circle radius. The number of defining elements used for the calculation by the present method is 30 and the submergence depth is two radii.

The effect on the lift and drag of the number of elements used to define the circle is of interest, since the accuracy of the present method is a function of this number. The following table presents values of lift and drag coefficients at a Froude number of 1·0 for circles described by 30, 60, 120 and 240 points and exact values calculated by Havelock (1936). The table shows a maximum error of 1·4 % for wave resistance but a slow convergence to higher accuracy as the number of points increases. The values of lift coefficient calculated by the present method,

seem to be converging to a value displaced 3 % from that calculated by using Havelock's formulas. This difference is probably due to inaccuracies in Havelock's values.

A recent attempt to test thin hydrofoil theory was carried out in Norway by Walderhaug (1964). A series of experimental tests was undertaken to determine

Number of defining elements	30	60	120	240	Havelock† exact
C_R	2·1082	2·0671	2·0753	2·0891	2·0948
C_L	1·0826	1·0759	1·0740	1·0795	1·1124

TABLE 1. Forces on a circular cylinder at $Fr = 1{\cdot}0$.

† Havelock's exact solution is actually a truncated series. The terms of the series are: $C_R = 1{\cdot}4461448 + 0{\cdot}45294412 + 0{\cdot}1781419 + 0{\cdot}02721836 - 0{\cdot}00965735$. $C_L = 0{\cdot}78984664 + 0{\cdot}24738609 + 0{\cdot}05410224 - 0{\cdot}00040036 + 0{\cdot}02143521$.

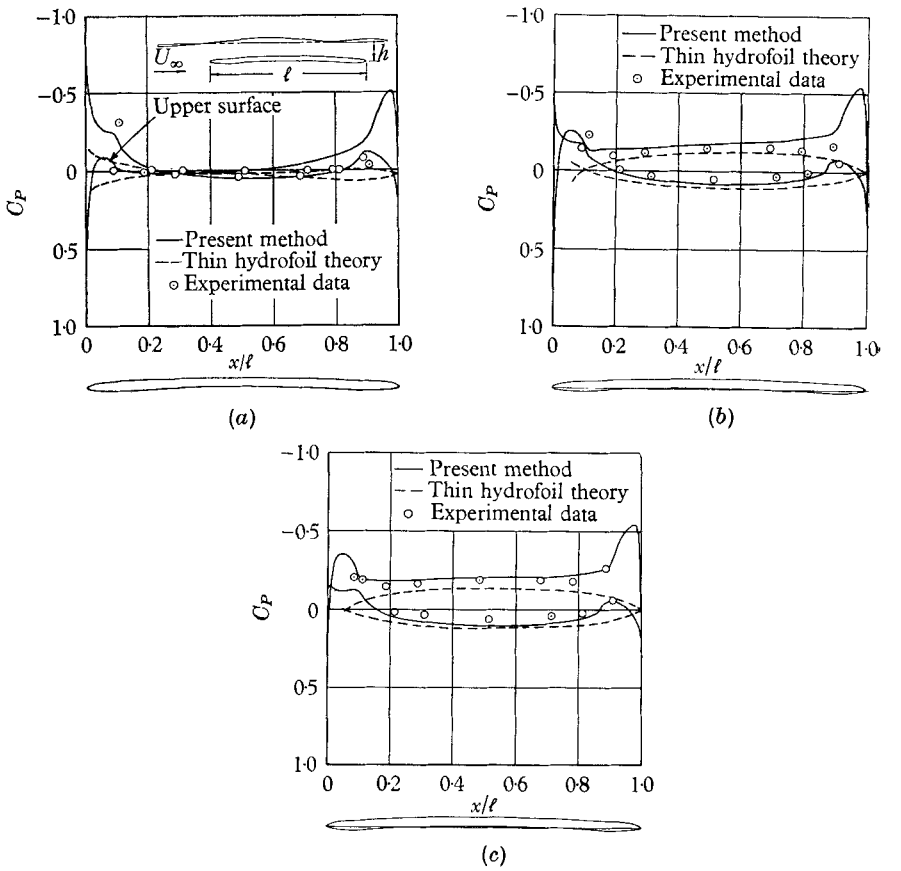

FIGURE 7. Comparison of the present method with thin hydrofoil theory and experimental data for various chord-line depths and Froude numbers. (*a*) $h/\ell = 0{\cdot}3$, $Fr = 0{\cdot}774$, $C_L = 0{\cdot}02$, $C_R = 0{\cdot}0072$. (*b*) $h/\ell = 1{\cdot}0$, $Fr = 1{\cdot}414$, $C_L = 0{\cdot}206$, $C_R = 0{\cdot}0058$. (*c*) $h/\ell = 2{\cdot}0$, $Fr = 2{\cdot}0$, $C_L = 0{\cdot}273$, $C_R = 0{\cdot}0041$.

pressure distributions on a 3% thick plate hydrofoil with an elliptic nose and trailing edge and a NACA 1.75-65 mean-line camber. This model was designed to closely approximate the camber-line hydrofoil model of Walderhaug's thin hydrofoil theory. Figures 7(*a*), (*b*) and (*c*) present Walderhaug's experimental and theoretical results and corresponding values calculated by the present method. Even for this case, the thin hydrofoil theory does not display the qualitative nature of the experimental pressure distribution. The results of the present method show small pressure peaks at the 10% chord and 90% chord locations. These are caused by a discontinuity in surface curvature at the points where the elliptic leading and trailing edges join the parallel sides of the hydrofoil.

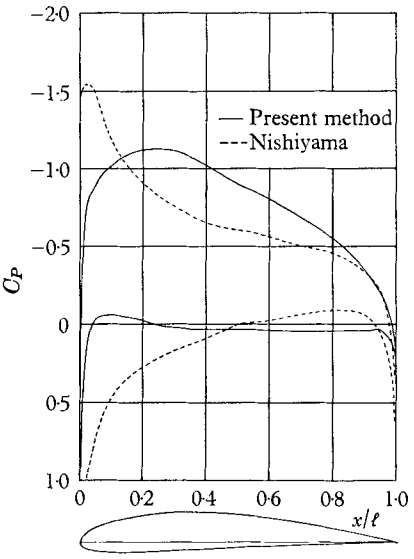

FIGURE 8. Comparison of the present method with the theory of Nishiyama (1957) for a NACA 4412 hydrofoil operating at $Fr = 1{\cdot}0$, $\alpha = 5°$, and mid-chord depth $h/\ell = 1{\cdot}0$.

Nishiyama (1957) has developed a theory for thick hydrofoils. In this theory the boundary condition on the body is satisfied by conformal mapping techniques. Figure 8 shows a comparison of calculations by the present method and calculations by Nishiyama for a 4412 hydrofoil. The pressure distributions are qualitatively different. An experimental investigation of the same airfoil was carried out by Ausman (1954); some of the results are presented in figures 9(*a*) and (*b*). The conditions under which the experimental values were taken for figure 9(*a*) are nearly the same as those for figure 8, and therefore the pressure distributions should be in qualitative agreement. Comparison of these figures verifies this kind of agreement between the experimental pressure distribution and the pressure distribution calculated by the present method. The reason for the discrepancy between the latter and Nishiyama's results is not known.

Also shown in figures 9(*a*) and (*b*) are results calculated by the present method for the exact conditions of the experiment. The experimental values lie below the potential or calculated values at equal values of angle of attack. This is to be expected, since the boundary-layer displacement effect lowers the circulation and

thus the minimum pressure. Also shown in figures 9 (*a*) and (*b*) are the more conventional comparisons at equal values of lift. As is to be expected, the agreement between the calculated and experimental results is better when the two are compared at equal values of lift.

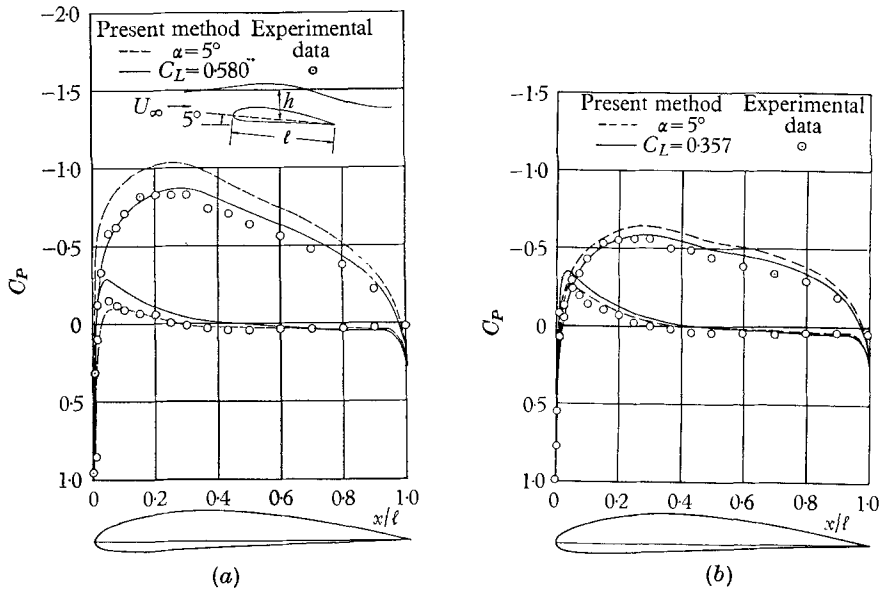

FIGURE 9. Comparison of calculated and experimental pressure distributions on a NACA 4412 hydrofoil at equal angles of attack and at equal lift coefficients for various mid chord depths at $Fr = 1{\cdot}03$. (*a*) $h/\ell = 0{\cdot}94$, $\alpha = 5°$, $C_L = 0{\cdot}58$. (*b*) $h/\ell = 0{\cdot}60$, $\alpha = 5°$, $C_L = 0{\cdot}357$.

The experiments conducted by Ausman were undertaken to show that the pressure on the upper surface of a hydrofoil is governed by hydrostatic conditions in addition to hydrodynamic conditions. Subsequent to Ausman's experiments, Laitone (1954) published a theory consistent with Ausman's experimental data that suggests that the minimum pressure on the hydrofoil is related to the maximum depth that can be produced by a hydraulic jump. Specifically, the theory states that the minimum pressure coefficient can be no less than $-(h/\ell)/Fr^2$. Laitone assumes that the height of the free surface, reduced by fluid flow over the shallow hydrofoil, is restored to its original height only by a hydraulic jump. Parkin, Perry & Wu (1955) have shown this to be true only at low Froude numbers and shallow depths. The hydrodynamical theory loses accuracy when a hydraulic jump appears above the hydrofoil, because the free-surface boundary has taken on a highly non-linear shape in the immediate vicinity of the hydrofoil. Since the hydrofoil is very near the free surface, the errors induced by the free-surface non-linearity have no chance to decay with depth.

Figures 10 (*a*) and (*b*) show to what extent the hydrodynamical theory holds even when the depth and Froude number are small. Figure 10 (*c*) shows two cases where a hydraulic jump has occurred above the hydrofoil. The hydrodynamic theory as calculated by the present method is inaccurate for this case, as is to be expected. The limiting negative pressures for the cases presented in figure 10 (*c*), as

calculated according to the theory of Laitone, are $-6{\cdot}92$ and $-11{\cdot}8$ for Froude numbers of 0·604 and 0·462, respectively. These numbers seem to bear little relation to the pressure distribution except that the experimental results do indeed lie below these limiting values. In figure 10, only the upper surface pressures are shown, since they are all that were measured. The data were taken

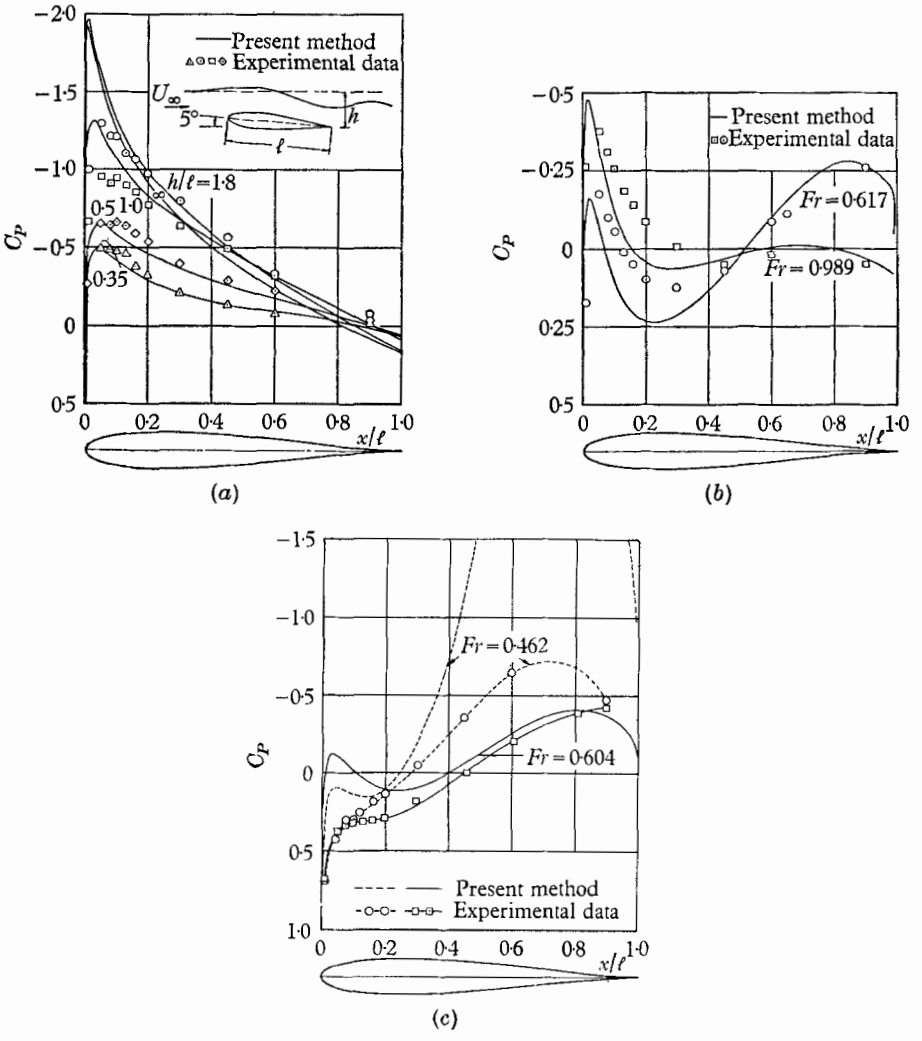

FIGURE 10. Comparison of calculated and experimental pressure distributions on the upper surface of a 12 % thick symmetric Joukowski hydrofoil at 5° angle of attack. (*a*) $Fr = 0{\cdot}95$, several values of h/ℓ. (*b*) $h/\ell = 0{\cdot}20$, two values of Fr. (*c*) $h/\ell = 0{\cdot}25$, two values of Fr.

from the experimental work of Parkin *et al.* (1955) for a 12 % thick symmetric Joukowski hydrofoil. Figure 10(*a*) exhibits one peculiarity. Near the hydrofoil nose there is a flattening of the experimental pressure peaks, for all cases, that cannot be explained by hydrostatic effects, viscous effects, or cavitation effects. This flattening persists even to the depth of 1·8 chords, which, for practical purposes, is close to infinite depth. The analytic result is shown in figure 10(*a*) for infinite

depth. It can be seen that the calculation made by the present method for a trailing edge depth of 1·8 chords is in better agreement with the analytic result than the experimental result is.

Further examples

In order to illustrate the capabilities of the present method, several calculations involving multiple bodies are presented. One example, the airfoil with slot and flap shown in figure 4, has already been mentioned. In the example the depth is infinite. However, the flow field can be calculated for any depth.

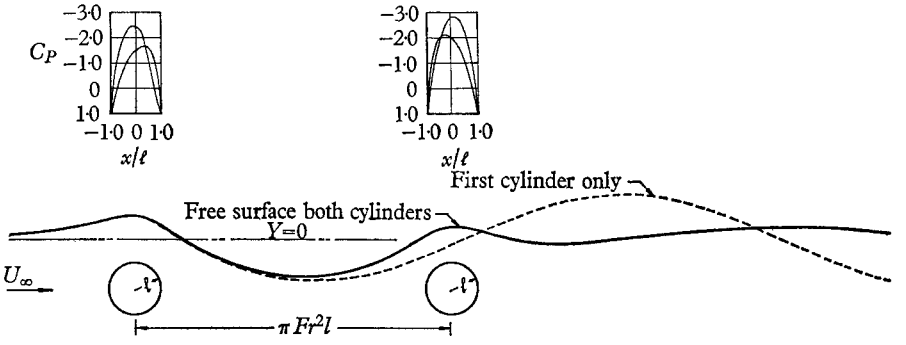

FIGURE 11. The pressure distributions and wave systems for two tandem circular cylinders operating at $Fr = 2{\cdot}0$, centre depths = 2 radii, $C_{R_1} = 0{\cdot}33$, $C_{R_2} = -0{\cdot}30$, $C_{R_{\text{total}}} = 0{\cdot}03$, $C_{L_1} = -0{\cdot}677$, $C_{L_2} = -0{\cdot}59$.

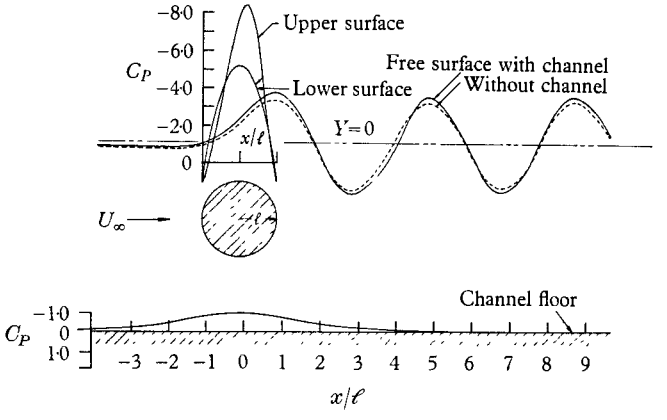

FIGURE 12. The pressure distribution and wave system for a circular cylinder operating at $Fr = 0{\cdot}80$ in a channel. Also shown is the pressure distribution along the channel floor. Circle centre depth = 2 radii, channel floor depth = 5 radii, $C_L = 2{\cdot}04$, $C_R = 1{\cdot}19$.

Figures 11 and 12 present two additional examples of multiple bodies. Figure 11 presents the pressure distribution and linear free-surface displacement for two circular cylinders of unit radius in tandem. The free-surface displacement for a single circle is also shown. The drag of the system of two circles is approximately one-tenth the drag of a single circle. This reduction in drag is caused by a cancellation of the trailing-wave system of the first circle by that of the second.

The distance between the two circles was selected as the distance between two dipoles whose wave trains cancel to zero.

Figure 12 presents the pressure distribution and linear free-surface displacement for a circle in a channel of finite depth. Since the present method was developed for a fluid unbounded in depth, the channel was simulated by simply placing a plane wall, 80 radii in length, as a second body in the infinitely deep fluid. The figure also shows that the wave effects have been reduced by the depth to the extent that the pressure distribution over the channel floor does not show the presence of the waves.

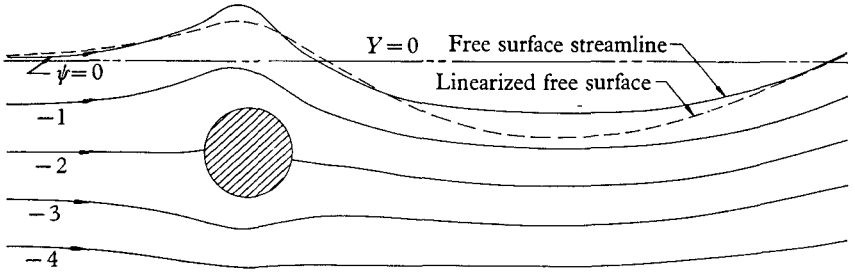

FIGURE 13. Streamlines for a circular cylinder operating at $Fr = 2{\cdot}0$, centre depth = 2 radii.

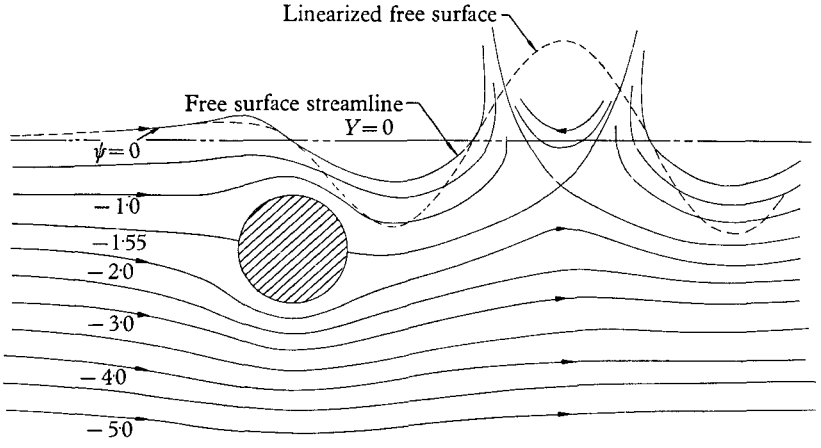

FIGURE 14. Streamlines for a circular cylinder operating at $Fr = 1{\cdot}0$, centre depth = 2 radii.

As is stated in the theory, the velocity at any point can be determined once the surface source strength and cyclic constants are known. Figure 13 presents the streamline pattern developed by a circular cylinder under a free surface. The streamlines were obtained by numerical integration of the velocity field. It can be seen that the free-surface streamline does not correspond exactly to the linear free-surface displacement. In extreme cases the streamline pattern may become quite unrealistic, as was recently shown by Tuck (1965). Tuck plotted the streamlines for a dipole under a free surface. In this case the dipole represents only an approximation of a circular cylinder. The same calculation was made for a

circular cylinder by the present method, and analogous results were obtained (see figure 14).

Work presented here was conducted by the Douglas Aircraft Company, Inc., Aircraft Division, under company-sponsored Research and Development Funds.

REFERENCES

AUSMAN, J. S. 1954 Pressure limitation on the upper surface of a hydrofoil. Ph.D. thesis in Mechanical Engineering at the University of California, Berkeley, California.

COOMBS, A. 1950 The translation of two bodies under the free surface of a heavy fluid. *Proc. Camb. Phil. Soc.* **46**, 453–468.

GIESING, J. P. 1966 Two-dimensional airfoil methods. *Douglas Aircraft Company Rept.* LB 31946.

HARRIS, T. A. & LOWRY, J. G. 1942 Pressure distribution over an NACA 23012 Airfoil with a fixed slot and slotted flap. *NACA Rept.* no. 732.

HAVELOCK, T. H. 1928 The vertical force on a cylinder submerged in a uniform stream. *Proc. Royal Soc.* A **122**, 387–393.

HAVELOCK, T. H. 1936 The forces on a circular cylinder submerged in a uniform stream. *Proc. Royal Soc.* A **157**, 526–534.

HESS, J. L. & SMITH, A. M. O. 1964 Calculation of non-lifting potential flow about arbitrary three-dimensional bodies. *J. Ship Res.* **8**, no. 2, 22–44.

HESS, J. L. & SMITH, A. M. O. 1966 Calculation of Potential Flow about Arbitrary Bodies. To be published in Progress in Aeronautical Sciences. Editor, D. Kucheman. Oxford & New York: Pergamon Press. Vol. 8

ISAY, W. H. 1960 Zur Theories der nahe der Wasseroberflaeche fahrenden Tragflaechen. *Ingenieur-Archiv, XXLX Band*, 295–313.

KELDYSCH, M. W. & LAWRENTJEW, M. A. 1935 On the motion of a wing below the surface of a heavy fluid. *ZAHI Paper, Moscow.*

KOCHIN, N. E. 1937 On the motion of profiles of any form below the surface of a heavy fluid. *ZAHI Paper, Moscow.*

KOCHIN, N. E., KIBEL, I. A. & ROZE, N. V. 1964 (Boyanovitch, D., Trans.) *Theoretical Hydromechanics*, 475–490. New York, London, Sydney: Interscience Publishers.

LAITONE, E. V. 1954 Limiting velocity by momentum relations for hydrofoils near the surface and airfoils in near sonic flow. *Proceedings of Second U.S. National Congress of Applied Mechanics*, pp. 751–754.

LAMB, H. 1932 *Hydrodynamics.* Cambridge University Press.

NISHIYAMA, TATSUO 1957 Study on submerged hydrofoils. *Society of Naval Architects of Japan, 60th Anniversary Series*, **2**, 95–134.

PARKIN, B. R., PERRY, B. & WU, T. Y. 1955 Pressure distribution on a hydrofoil running near the water surface. *Calif. Inst. of Tech. Hydrodynamics Lab. Rept.* no. 47-2.

SMITH, A. M. O., GIESING, J. P. & HESS, J. L. 1963 Calculation of waves and wave resistance for bodies moving on or beneath the surface of the sea. *Douglas Aircraft Company Rept.* LB 31488.

SMITH, A. M. O. & PIERCE, JESSE 1958 Exact solution of the Neumann problem. Calculation of non-circulatory plane and axially symmetric flow about or within arbitrary boundaries. *Douglas Aircraft Company Rept.* ES 26988.

TUCK, E. O. 1965 The effect of non-linearity at the free surface on flow past a submerged cylinder. *J. Fluid Mech.* **22**, 401–414.

WALDERHAUG, H. A. 1964 On the chordwise pressure distributions on submerged hydrofoils. *Norwegian Ship Model Experiment Tank Publication* no. 75.

WEHAUSEN, J. V. & LAITONE, E. V. 1960 *Handbook of Physics*, **9**, *Surface Waves.* Berlin: Springer-Verlag.